Original Paper

High-Resolution Quasi-3D Electric Resistivity Tomography for Deciphering Groundwater Potential Zones in Lateritic Terrain

Rupesh,[1] Prarabdh Tiwari [iD],[1,2] and S. P. Sharma[1]

Groundwater is under constant threat of exploitation with increasing demands. Therefore, there is a need for more advanced methods for exploring potential groundwater zones to meet people requirements. Groundwater in hard terrain areas is present in fractured zones, whereas in lateritic terrain it occurs in layered strata. Electrical resistivity tomography (ERT) is an advanced geophysical technique used in our present study; a quasi-3D ERT survey was conducted using different arrays. 2D Geophysical data were acquired along 18 ERT profiles of Wenner and Wenner–Schlumberger arrays and 13 ERT profiles of Dipole–Dipole array. Each profile of 200 m length was kept parallel to each other at 5 m spacing in the E–W direction. The inverted response was generated and, based on resistivity distribution, different geological layers of clay, sand and laterite were delineated using various ERT arrays. A conductive zone was marked as a potential aquifer zone at depths of 7–10 m below ground level. Thus, the quasi-3D geoelectrical approach was applied successfully in a lateritic environment for deciphering potential groundwater zones.

KEY WORDS: Groundwater, Electrical resistivity tomography, Aquifer, Laterite, 2D and 3D inversion.

INTRODUCTION

Electrical resistivity tomography (ERT) is a geophysical technique that can delineate and characterize subsurface features. It works as an imaging tool for the resistivity contrast of the subsurface. Electrical resistivity methods are applied successfully in hydrogeology (Sandberg et al., 2002), mining engineering (Zhang et al., 2009), archaeology (Noel & Xu, 1991), and civil engineering (Castilho & Maia, 2008) fields. Many authors contributed their research work to solve the issues related to complex geology areas (Griffiths & Barker, 1993), environmental application (Dahlin et al., 2002), Groundwater investigation (AL-Garni et al., 2005; Arkoprovo et al., 2012, 2013; Aziz et al., 2019; Bharti et al., 2019; Chandra et al., 2006; Daily et al., 1992; Kumar et al., 2014, 2016). Groundwater plays a significant role in sustaining human beings and other living objects. Out of all water available on the earth's surface, groundwater accounts for only 0.60% (Raghunath, 2006). The role of groundwater role becomes essential in areas where additional water source is not available, especially in complex geology, drought-prone areas, and problematic rock areas where people are suffering due to lack of water.

Out of all the geophysical methods, electrical resistivity methods are used mainly for groundwater

[1]Department of Geology and Geophysics, Indian Institute of Technology Kharagpur, Kharagpur, West Bengal 721302, India.
[2]To whom correspondence should be addressed; e-mail: pt.tiwari75@gmail.com, prarabdh@iitkgp.ac.in

exploration. Vertical electrical sounding takes into account only 1-D changes in resistivity. In contrast, electrical resistivity imaging technique measures resistivity changes in the vertical and horizontal directions with the presumption that it does not change perpendicular to the profile line direction (Dey & Morrison, 1979; Gharibi & Bentley, 2005; Griffiths & Barker, 1993; Griffiths et al., 1990; Koefoed, 1979; Loke & Barker, 1996; Park & Van, 1991; Storz et al., 2000; Yi et al., 2001). This limitation is overcome by 3D ERT (Loke, 1999). 2D inversion is insufficient for mapping the three-dimensional inhomogeneity encountered in the subsurface. 3D inversion is more efficient than 2D in eliminating spurious features and increasing the reliability of inversion images (Loke, 2004; Park et al., 2016). The present study deciphers mainly potential groundwater zones in lateritic terrain using quasi-3D ERT with different electrode configurations.

Laterite is one of soil type that is rich in iron and aluminum. Nearly all laterites are red because of iron oxide (Tardy, 1992, 1997; Usifo et al., 2018). Layers of laterite are typically thick, porous, and impermeable. In hard rock areas, groundwater is present in fracture zones. In lateritic terrain, groundwater is present in layered strata. However, it is challenging to map groundwater flow in 2D. Thus, in this area, a quasi-3D ERT survey was planned. Correct mapping of subsurface water is an essential demand for protecting human beings and the environment. By proper mapping and systematic study of the site, water scarcity can be solved through artificial recharge in water scarcity zones.

GEOLOGICAL SETTING OF THE STUDY AREA

The study area is in Paschim Medinipur District. It lies between 21° 46′ N and 22° 57′ N latitudes and between 86° 33′ E and 87° 44′ E longitudes. The study area lies to the south of the tropic of cancer, and climatologically, it falls in the Gangetic West Bengal. The study area, which is drained by the rivers flowing from the Bihar plateau, includes the towns of Subarnarekha, Haldi, Kasai, Kalighai, Rupnarayan, Rasulpur, Damodar, and Hooghly. It covers an area of 9081.13 km^2 (Bhunia et al., 2012). The district's average temperature varies widely across seasons, ranging between a maximum of 43 °C with relatively high humidity and a minimum

of 7 °C with well-distributed rainfall during monsoon (Bhunia et al., 2012).

The region reveals primarily geological formations categorized from Proterozoic to Quaternary: fluvio–deltaic sediments, younger alluvium, older alluvium, platform margin conglomerate, and basement crystalline complex (Fig. 1). In the coastal plains of West Bengal, large areas of Quaternary surface formations exist. The city lies in the southwestern part of the Bengal geosynclinal basin (Sengupta, 1966). The Kharagpur upland is one of the geomorphic divisions of this area with a NNE–SSW trending belt, whose surface is masked by lateritic soil and represented by hard crust mottled clay soil. The age of this is considered middle Pleistocene (Niyogi, 1975). The laterite deposits in the study area were produced by lateralization of Quaternary alluvium.

The site at IIT Kharagpur (Fig. 2) is located 120 km west of Kolkata and it lies south of the Kasai River. The hard layer covers the Kharagpur area near the soil's surface. Ranges of layer thicknesses are from a few centimeters to several meters. The Kharagpur area is covered with low ridges and hills with red gravelly soil. Moderate groundwater potential zones and average drainage density are attributed to the previous study (Mondal, 2012). The site is covered, from the top of the surface to a depth of 170.688 m, with laterite granules, laterite dust, and medium- to coarse-grained sand, silt, and clay. The soil types are identified from borehole data (Fig. 3). Two nearby boreholes, BH-1 (170.688 m depth) and BH-2 (201.168 m depth) are present in the study area (Mukherjee & Sengupta, 2014). BH-2 (Fig. 3) is situated near the ERT survey area. It shows the presence of lateritic granules up to 6 m in depth. The basement complex in the study area is found as low recharge and poor storage groundwater zone (Chowdhury et al., 2009).

METHODOLOGY

Nowadays, ERT is used generally for delineating potential groundwater zones. It is an active geophysical method in which direct current or low-frequency alternate current injected into the ground. The required input signal generated from the battery was used for measuring the apparent resistivity of the subsurface. The ERT was carried out using a multi-electrodes (41) system in which electrodes were placed at equal distance and measuring the
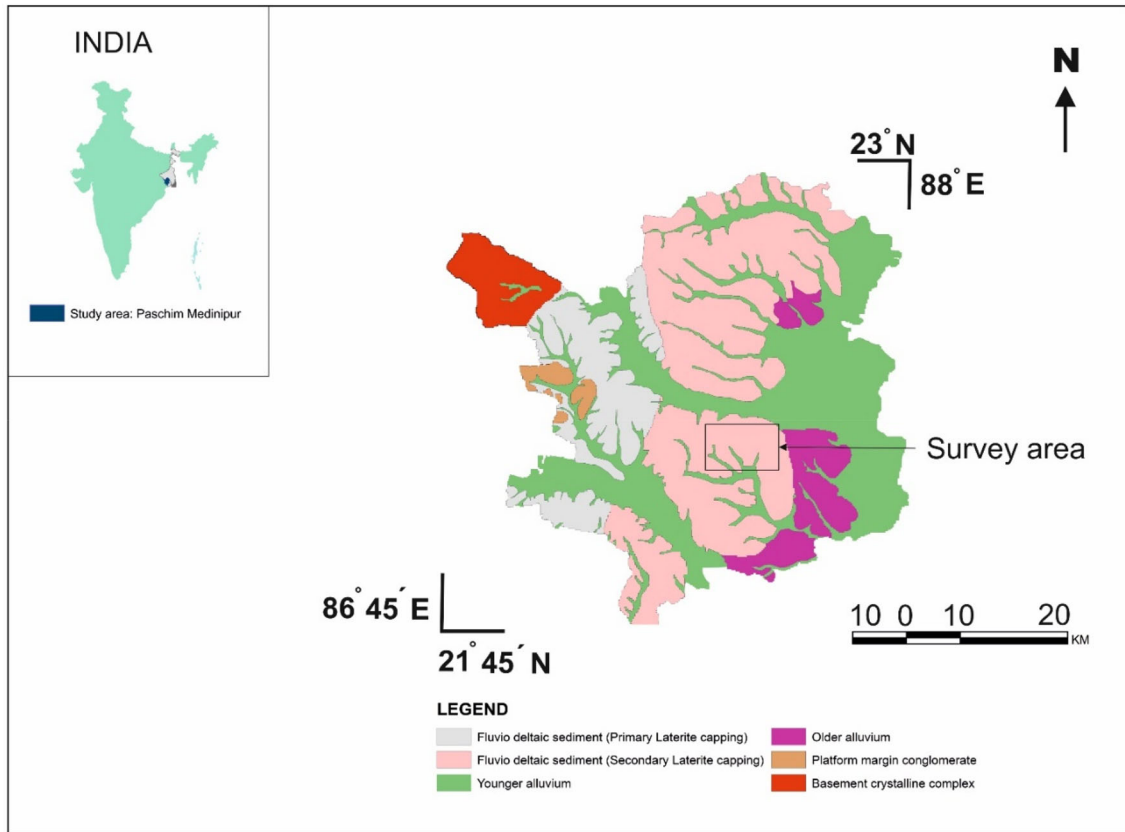
Figure 1. Geology of the study area (modified after Chowdhury et al., 2009).

resistivity variation corresponding to the subsurface. Different arrays were used for ERT data acquisition (Fig. 4). The distance between the consecutive electrodes and parallel profiles was 5 m.

Apparent resistivity values (in ohm-m) were calculated as (Telford et al., 1990):

$$\rho_a = k\frac{\Delta V}{I} \tag{1}$$

where ρ_a is apparent resistivity, ΔV is measured potential difference (in volt), I is current (in ampere), and k is the geometric factor. For Wenner array, $k = 2\pi a$. For Wenner–Schlumberger array. $k = \pi na(n+1)$. For Dipole–Dipole array, $k = \pi na(n+1)(n+2)$ where a is the distance between electrodes.

We took 18 profiles of 5 m interval each at site location (Fig. 5). Measurements were done for Wenner, Wenner–Schlumberger, and Dipole–Dipole arrays to see the horizontal and vertical variation of resistivity within the study area. All the profiles were taken side by side from the east to the west direction. The area covered for quasi-3D data measurement was 200 m × 85 m. The data acquisition strategy was to get the maximum resolution to interpret subsurface features in the lateritic area. The spacing between each profile and between each electrode along the profile was 5 m to reduce the banding effect in the 3D inversion model (Loke & Dahlin, 2010). The length of each profile was 200 m. ABEM LS resistivity imaging equipment and electrodes were connected through a multi-core cable. This equipment was user friendly; it makes measurement automatically. The position of current electrodes and potential electrodes depends on the geometry chosen by the user. This way, we measured the apparent resistivity values for Wenner, Wenner–Schlumberger, and Dipole–Dipole arrays (Dahlin, 2001; Kumar et al., 2020; Terrameter, 2012).

After the data acquisition, a program RES2DINV was used for the inversion of 2D data. The inverted model was involved in getting a true resistivity of the subsurface. Rectangular blocks in the model signify resistivity values. A program was used
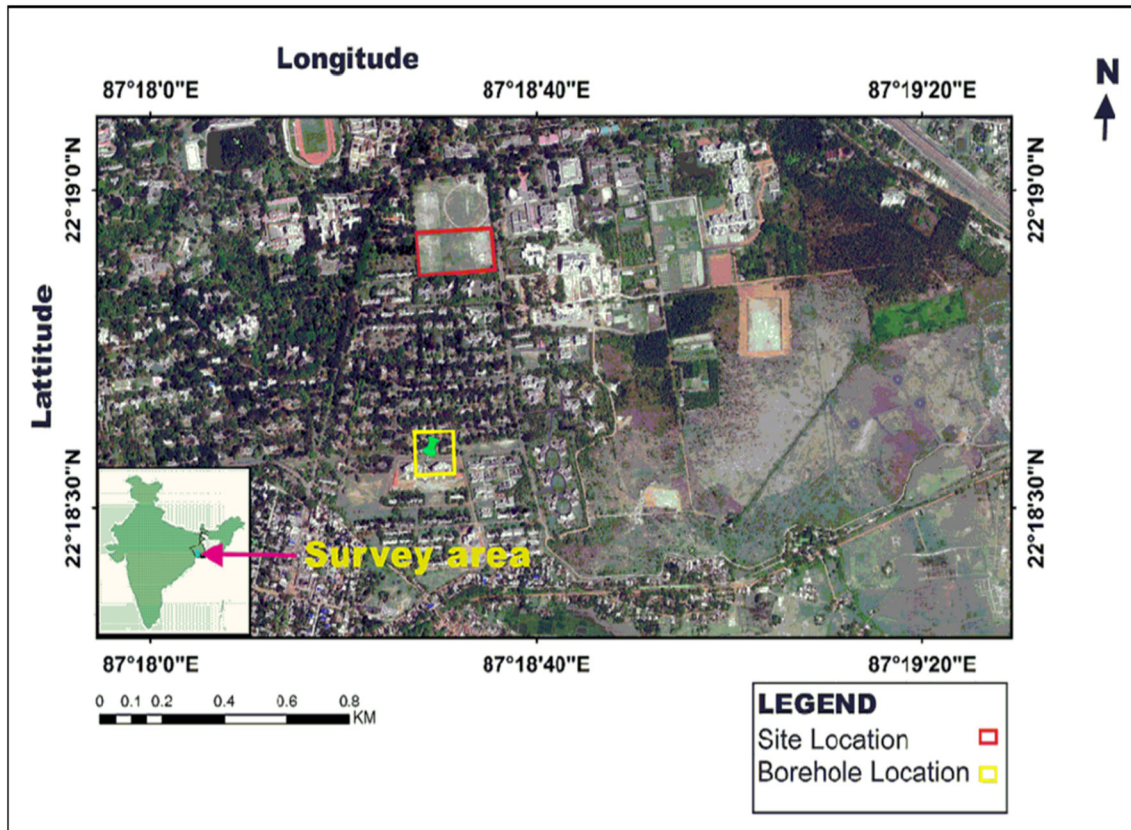
Figure 2. Google image showing the location of the study area in IIT Kharagpur (Paschim Medinipur).

to determine the blocks' resistivity. The apparent resistivity values and the electrodes' location were specified in a text file and perused by the RES2DINV program. The least-squares inversion method was used for the subsurface model.

For 3D inversion, the whole 2D data set was collated and converted into a 3D data set called quasi-3D. RES3DINV program was used for the inversion of quasi-3D data. Horizontal cross sections obtained from the inverted field data set were presented in the x and y planes. Inverted 3D data were used in the Para view (3D open-source software) to visualize the subsurface in three dimensions and to interpret the subsurface features based on resistivity contrast.

2D AND 3D INVERSION OF ERT DATA

We removed negative resistivity values, spikes, and bad data points before carrying out the inversion to obtain a correct model. RMS (root-mean-square) error statistics are shown in Figure 6 for collated 3D Wenner array. The smallest error is represented by the highest bar in the bar chart, and with increasing error, the bar's height decreases. The bad data points were due to poor contact of electrodes with the ground, break-in cable, and telluric current. Thus, such points were removed before any inversion process (Loke, 2004). After that, the inversion procedure was executed on the data set to achieve an optimum result.

RES2DINV and RES3DINV software packages were used for the smoothness constrained inversion method (de Groot-Hedlin & Constable, 1990; Loke, 2003; Sasaki, 1992). This method is generally used for inversion of 2D and 3D resistivity data. The purpose was to minimize the difference between measured and modeled data called data misfit. The inversion technique was applied to find a subsurface model whose response agrees with the measured data. It tries to reduce other quantities to improve the resulting model and stabilize the inversion process. The program attempts to find an improved model to reduce misfit error. The mathe-

matical form for the smoothness constrained inversion method is (Loke, 2004):

$$(J^T J + uF)d = J^T g - uFr \qquad (2)$$

where F is a smoothing matrix, J is a Jacobian matrix of partial derivatives, r is a vector containing the logarithm of the model resistivity values, u is the damping factor, d is a model perturbation vector, and g is a discrepancy vector. The g describes the difference between the calculated and measured apparent resistivity values. The discrepancy vector's magnitude gives a RMS value, and d express the change in the model resistivity values calculated using Eq. 2. This equation tries to minimize the difference between the calculated and measured apparent resistivity values. The damping factor u is for the model smoothness. If a more considerable value of the damping factor is taken, then the model
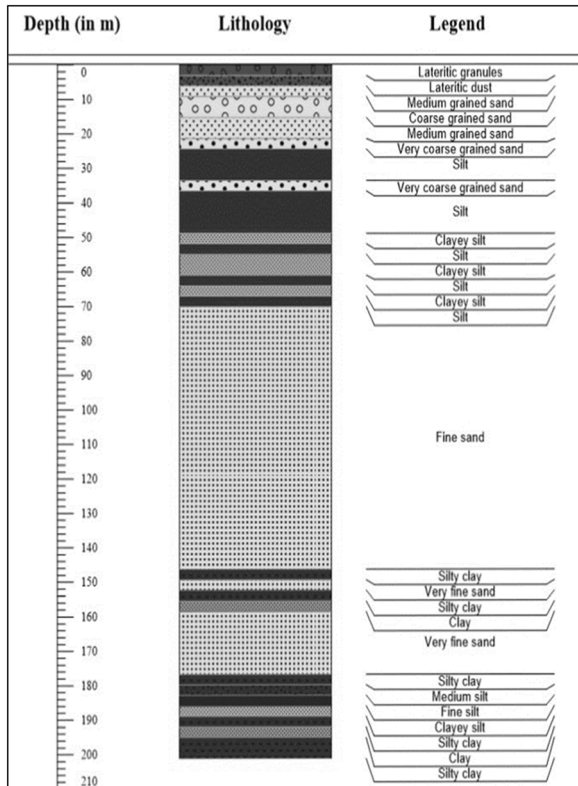

Figure 3. Borehole section shows soil type from top to 201.168 m depth (after Mukherjee 2014).
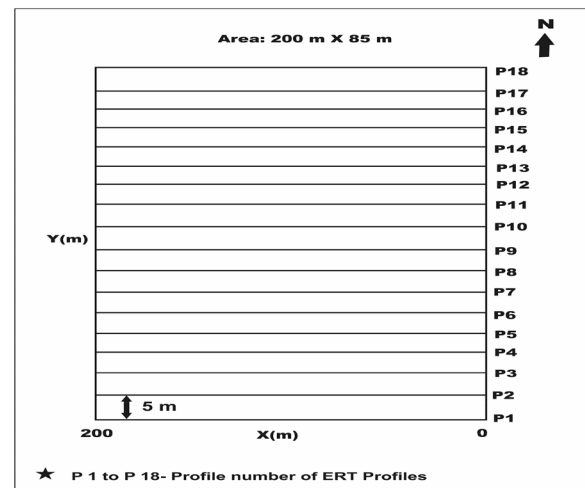

Figure 5. Layout showing parallel arrangement of ERT lines used for quasi-3D ERT acquisition in the Tata sports complex (IIT Kharagpur).
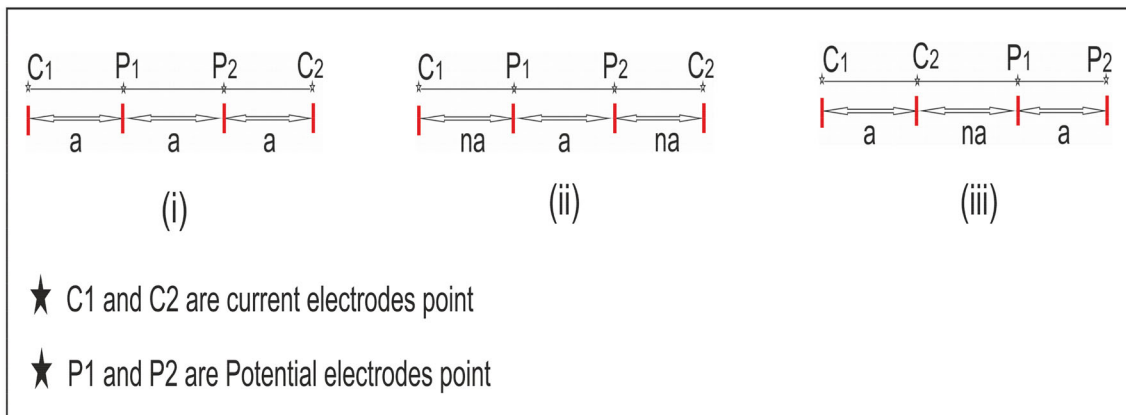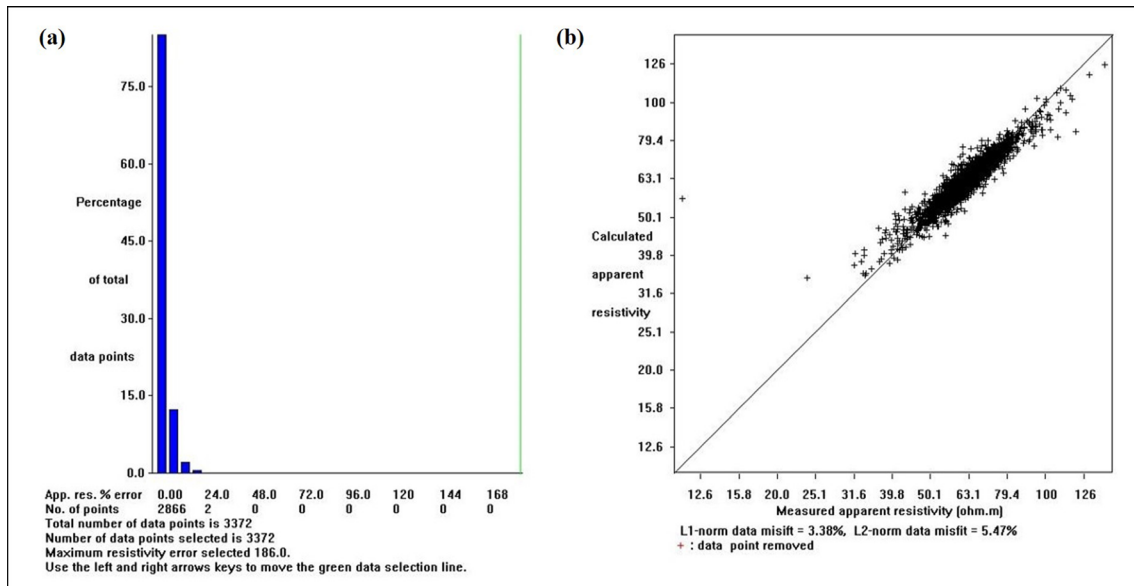

Figure 4. Electrode configuration for (**i**) Wenner array, (**ii**) Wenner–Schlumberger array and, (**iii**) Dipole–Dipole array.

Figure 6. (**a**) RMS error statistics for the 2d inversion scheme. (**b**) Plot of calculated vs. apparent resistivity values.

will be smoother, but the RMS error can be more prominent (Loke, 2004). In this study, 2D and quasi-3D inverted models were presented to produce images of the investigated site's subsurface structure within the campus of the IIT Kharagpur (Paschim Medinipur) West Bengal, India.

RESULTS AND INTERPRETATION

Wenner Array

Wenner array gives a high signal-to-noise ratio and good lateral resolution for layered structures in nature. However, as one goes down in-depth, signal strength will decrease, and resolution will reduce. After processing all collected profiles with Wenner array, pseudo-section for profile numbers P2 and P3 are presented in Figure 7. This figure shows that the Wenner array gives a good response for shallow depth of investigation in laterite terrain. Low resistivity (< 50 Ω-m) in blue in Figure 7 is interpreted as an aquifer. Laterites of high resistivity (> 90 Ω-m) are characterized by red and purple colors observed in the Wenner array's inverted model.

Inverted images from profiles 15 to 18 are displayed in Figure 8. Resistivity distribution in all these images is almost the same. In Figure 8, it is observed that laterites (impermeable layer) exist from the near-surface (6.0 m) to a depth of 19.0 m in the middle of the profile. Some signatures of water accumulation and water percolation are visible at the near-surface and at the eastern end and western end of the pseudo-sections.

In Figure 9, horizontal depth slices are displayed. The geoelectrical layers were divided into eight layers segment, with a depth range of 34.3 m. The first to eighth layers had thicknesses of 2.5 m, 2.88 m, 3.3 m, 3.82 m, 4.4 m, 5.0 m, 5.8 m, and 6.6 m. In the first layer, the lowest resistivity range of 14–30 Ω-m indicates water signatures. From layer one to layer five, resistivity range beyond 90 Ω-m represents lateritic soil. From the inference of borehole data (Fig. 3), the resistivity range 30–90 Ω-m in the entire layers segment gives the signature of medium- to coarse-grained sand and clay compositions.

The 3D models were plotted using Para view (open-source visualization). Figure 10 is a 3D diagram of the combined resistivity distribution of inverted resistivity data. This figure indicates variation
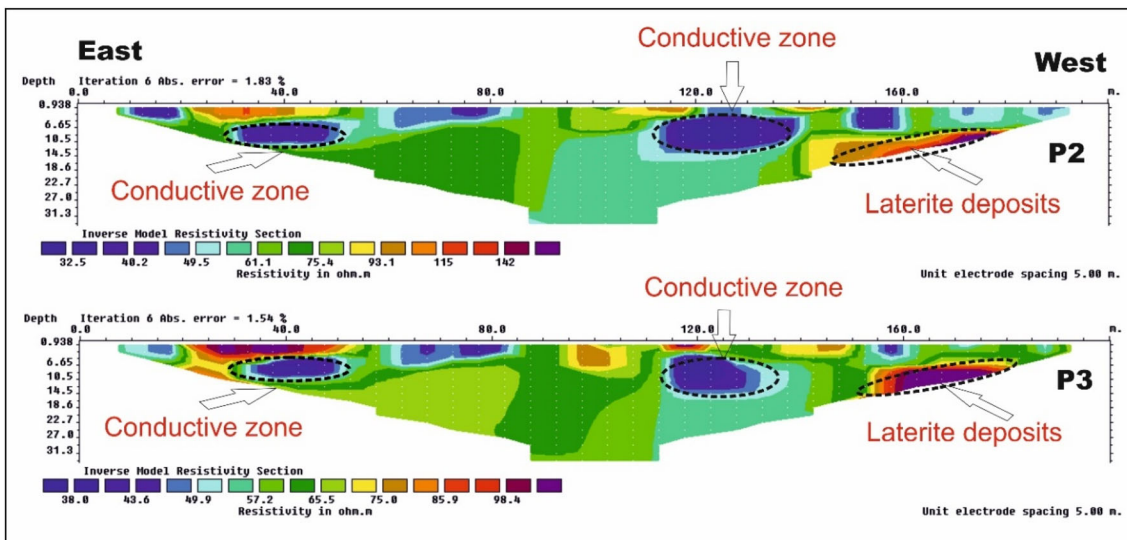
Figure 7. Two-dimensional resistivity inversion results (Wenner array: profiles 2 and 3).
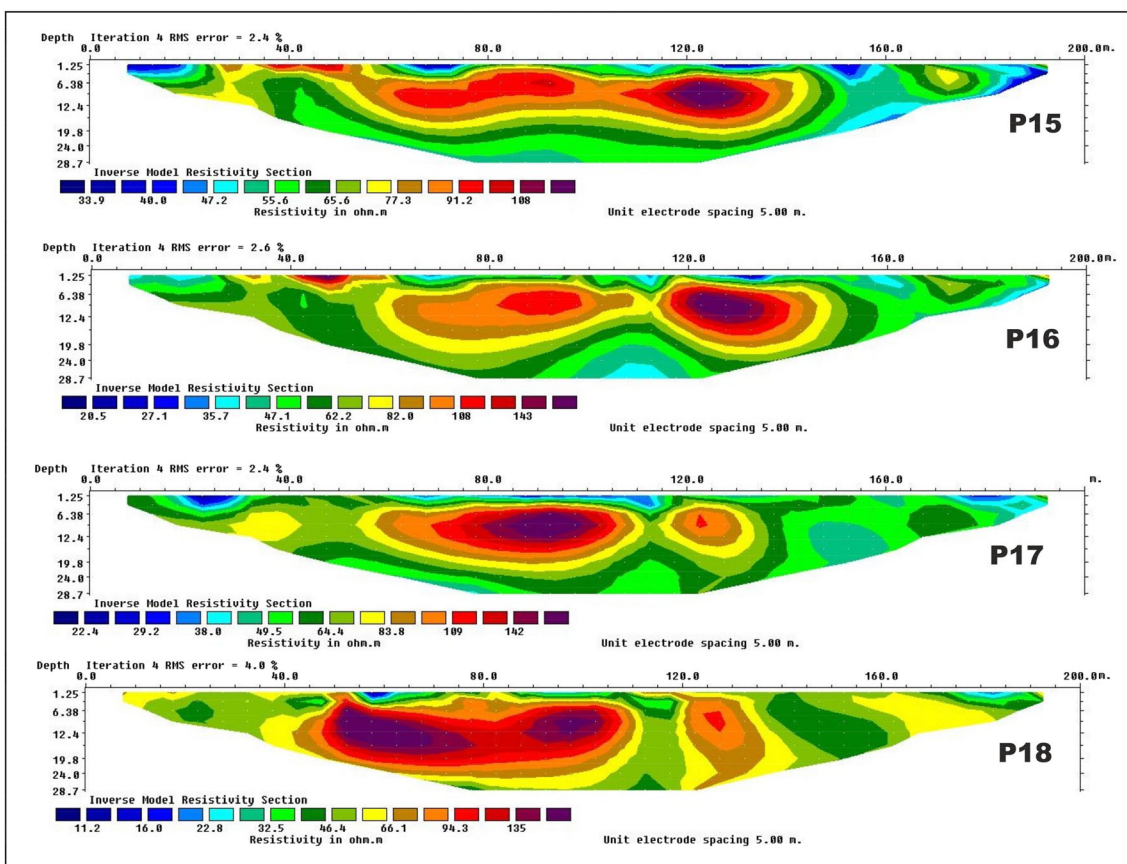

Figure 8. Two-dimensional resistivity inversion results (Wenner array: profiles 15–18).

in ground resistivity in the three orthogonal directions. Some profiles were taken during the running tap water (ground man giving water to sports ground). Its effect appears as low resistivity distribution on the surface; its connectivity with the aquifer can be seen in the 3D model of the Wenner array. The laterites zone of high resistivity and the aquifer of low resistivity were observed and marked in the image.

Wenner–Schlumberger Array

This is a composite technique of the Wenner and Schlumberger arrays and well known as the Wenner–Schlumberger array. The data points for this array are more than those in the Wenner array. This hybrid technique's signal strength is weaker than the Wenner array but higher than the Dipole–Dipole array. The 2D inverted results for profiles from P15 to P18 are displayed in Figure 11. In this figure, the imaging depth (33.8 m) exceeds that of the Wenner array. In the image of P1, laterite layer is clearly observed, but a picture of the other profiles shown in Figure 11 signifies laterite deposits are in patches. Subsurface water plume is observed from P16 to P17 in the blue color of low resistivity. The high resistivity region shows the presence of laterite deposits marked as red color in the 2d image.

3D inversion result for Wenner–Schlumberger array on the x and y planes is presented in Figure 12, where signatures of laterites are observed from layer one to layer five up to 16.9 m. Low resistivity distribution in all layers is irregular, and it is not correlated. Patches of water are seen only in the first layer but not in the other layers. After correlating with borehole data, the distribution of moderate to high resistivity values from layer 3 to layer 8 signifies the presence of fine sand to moraine sand.

Depth slices in a three-dimensional environment with quasi-3D Wenner–Schlumberger electrode configurations are displayed in Figure 13. Low resistivity is observed linearly in the x–y plane at the shallow surface. The zone of low resistivity in blue color with the same color contrast is observed at greater depth (z-axis) in the fourth and seventh slices, which signifies water percolating from near-surface to more profound depth. High resistivity zones in red color, which are interpreted as laterites, are observed in first to fifth slices with decreasing resolution.

The 3D model derived by using quasi-3D inverted data of the Wenner–Schlumberger array is presented in Figure 14. The resolution to interpret the features near the surface is not fair, as the Wenner 3D model is shown. The conductive zone present in the 3D model is interpreted as a probable aquifer zone. It is also observed that the overall resolution is fair but not the best in this image to interpret other features. The ambiguity in the 2D view of inverted images has been removed in three-dimensional visualization of subsurface resistivity distribution.

Dipole–Dipole Array

In the Dipole–Dipole array, signal strength is lower, and the horizontal coverage is narrower than the Wenner–Schlumberger array. The Dipole–Dipole electrode configuration is sensitive to lateral changes in resistivity. However, it can resolve satisfactorily the vertical structures compared to the horizontal anomaly present in the subsurface. The pseudo-sections for profile P15 to P18 are displayed in Figure 15. Laterite deposits (red color) shown in patches not as continuous as displayed in Wenner array's inversion result. A low resistivity anomaly is observed in all inverted profile images interpreted as water plume at the center of the profile in-depth section.

3D inversion result for Dipole–Dipole array on the x and y plane is shown in Figure 16, where signatures of laterites of high resistivity are observed in all layers. However, low resistivity appearances in blue color are observed from near-surface to layer five at 8.74 m depth. From the depth point of view, the resistivity values for water signatures increases. It may be because of the mixing of sand in water or the cumulative effect of host bodies.

Three-dimension representation of ground resistivity distribution displayed as a 3D model in Figure 17 for Dipole–Dipole array. In the Dipole–Dipole array, aquifer signature and laterite deposits are poorly resolved compared to the Wenner array.

DISCUSSION

The study incorporates the quasi-3D ERT data acquisition for exploring the groundwater zones in a lateritic environment. We have found the substantial signature of conductive zones beneath the subsur-
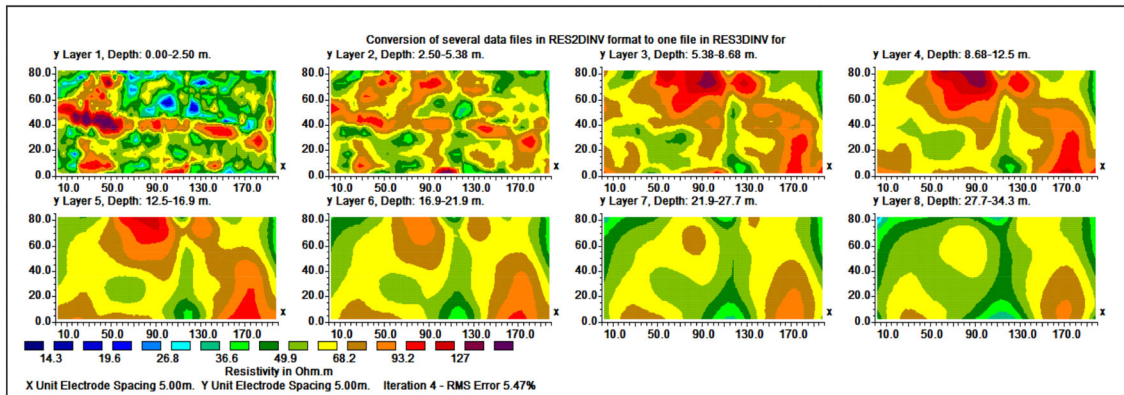
Figure 9. Three-dimensional resistivity inversion results (Wenner array) on the *x*, *y* plane (from 0 to 34.3 m depth).
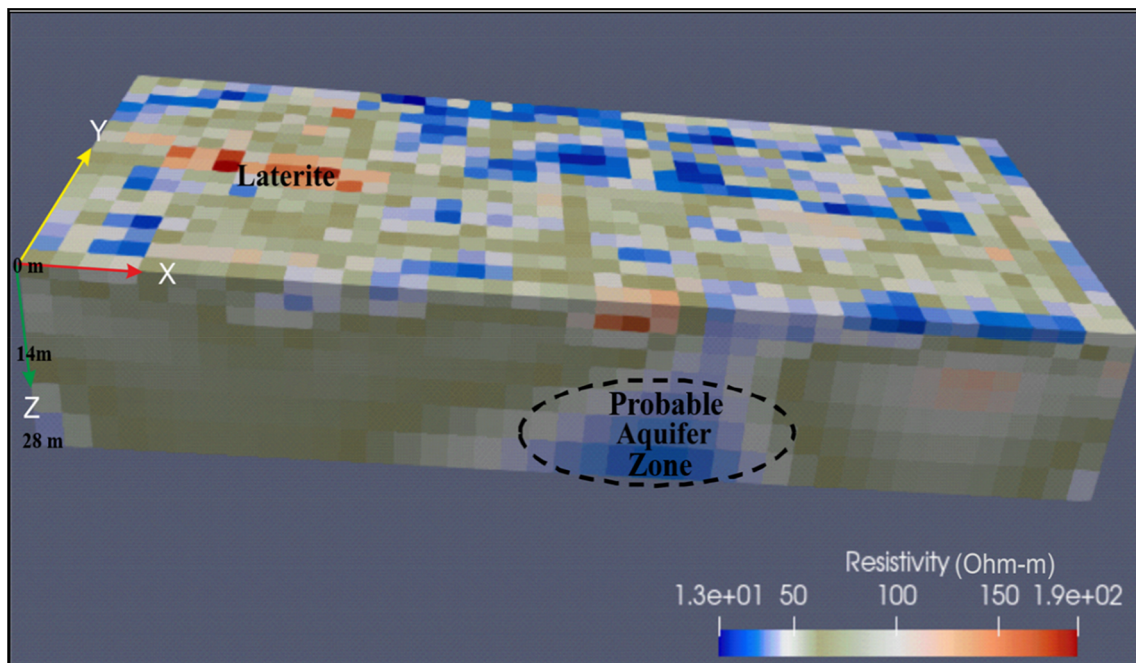

Figure 10. Three-dimensional subsurface model (*x*, *y*, and *z* directions) showing resistivity variations for the Wenner array.

face. Using borehole data information, these conductive zones are interpreted as aquifer zones of clay to sand signature. From inversion results, these zones are well delineated in the 2d as well as 3d images of the different array. The previous study in this area (Panda et al., 2018) found different geological layers based on resistivity obtained from sounding data, as clay (20 Ω-m), sand (15–40 Ω-m) and laterite (120–192 Ω-m). According to their study, laterites can be problematic for the infiltration of rainwater. However, their study was limited to

exploring the lateral extension of laterites, as they have used only 2D geophysical investigation. However, from the present quasi-3D survey, the subsurface geological layers of clay, sand, laterite are well resolved. In this study, similar ranges of resistivity values were found for clay (20–30 Ω-m), sand (30–45 Ω-m) and semi-permeable to impermeable laterite deposits (350–1000 Ω-m).

The Wenner array provides the most substantial signal strength, and it helps resolve horizontal structures. It is observed that the Wenner
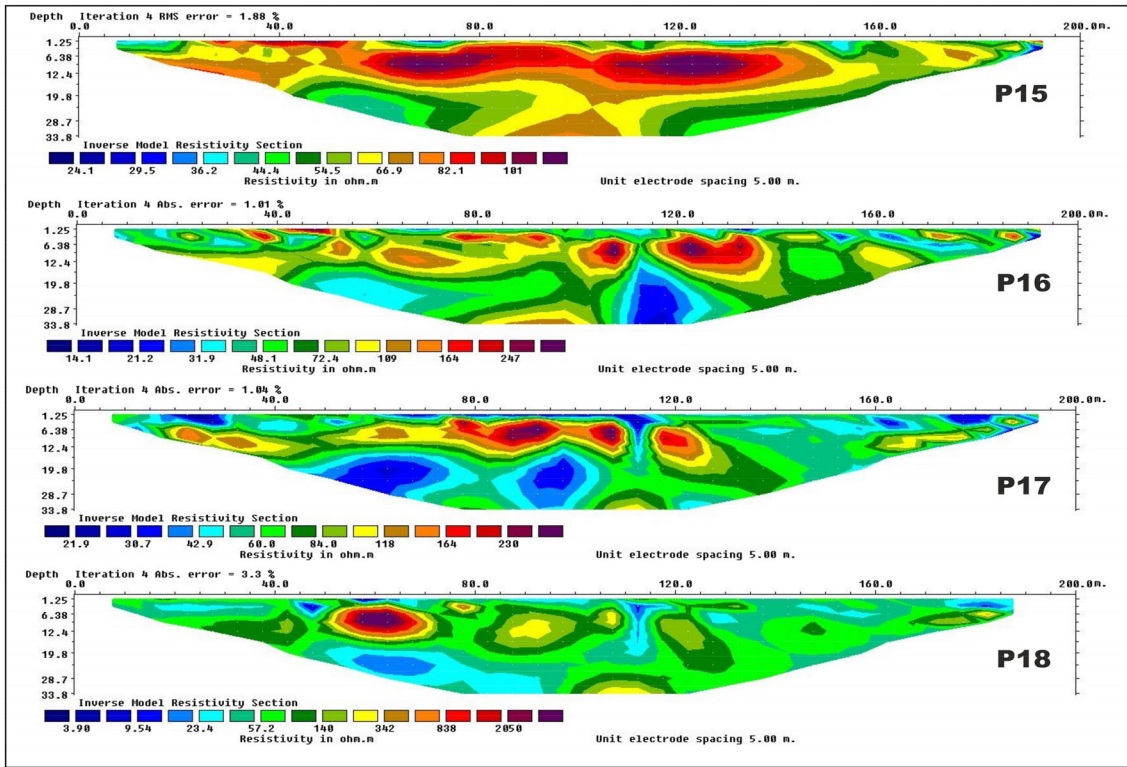
Figure 11. Two-dimensional resistivity inversion results (Wenner–Schlumberger array: profiles 15–18).
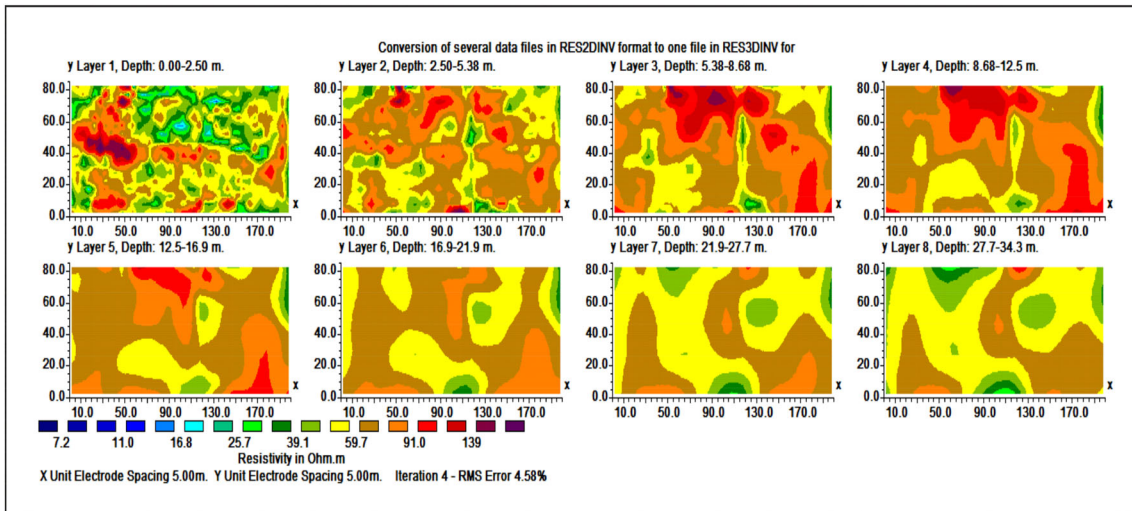

Figure 12. Three-dimensional resistivity inversion results (Wenner–Schlumberger array) on the x, y plane (from 0 to 34.3 m depth).

array has resolved shallow aquifer zones and laterite deposits significantly as compared to the other arrays. In the Wenner–Schlumberger array, the investigation depth was much greater than the Wenner array. The laterite and water signatures in this array were seen in patches. The Dipole–Dipole
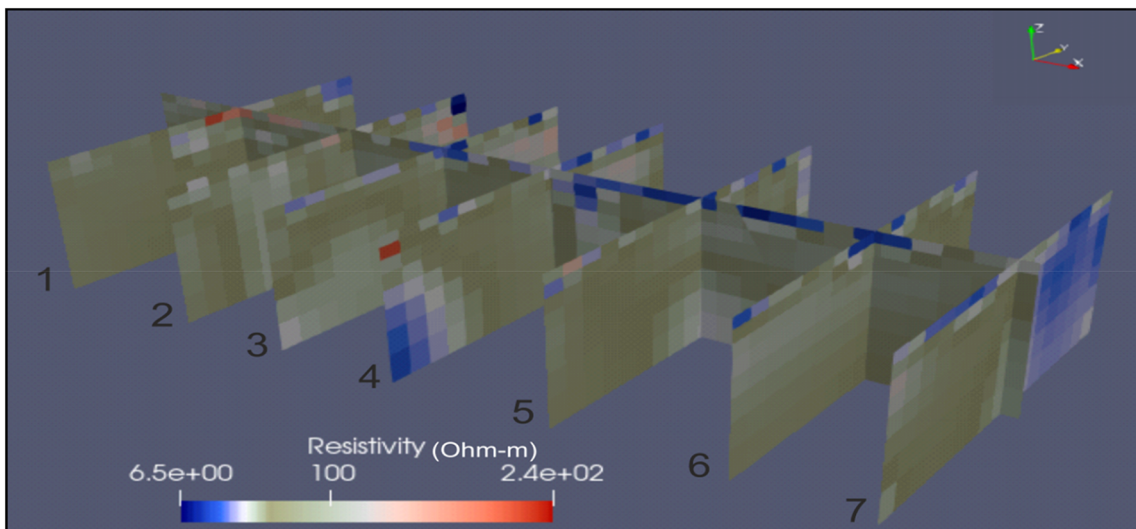
Figure 13. Depth slices in three-dimensional environment (x, y, and z directions) showing resistivity variations for the Wenner–Schlumberger array.
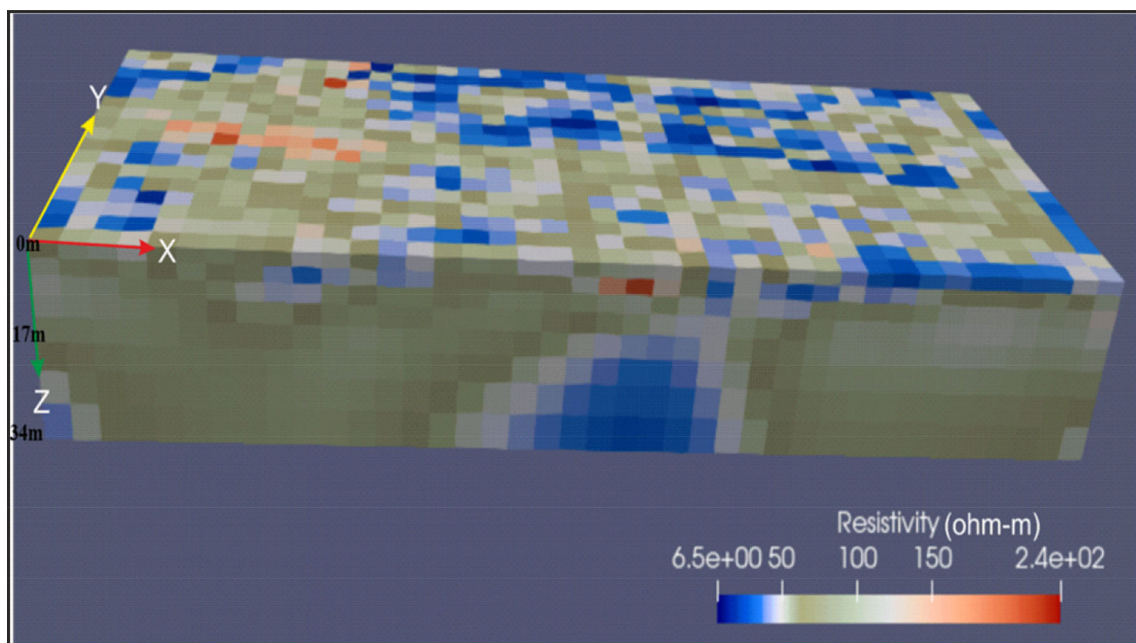

Figure 14. Three-dimensional model (x, y, and z directions) showing resistivity variations for the Wenner–Schlumberger array.

array was very sensitive to vertical structures but not so for horizontal structures. Hence, the laterite layer appeared in patches irregularly, and the water plume extended into greater depth compared to the other arrays used in the study. Depth slices in three-dimensional environments with Wenner–Schlumberger array showed water percolation from near-surface to the aquifer zone. The 3D model
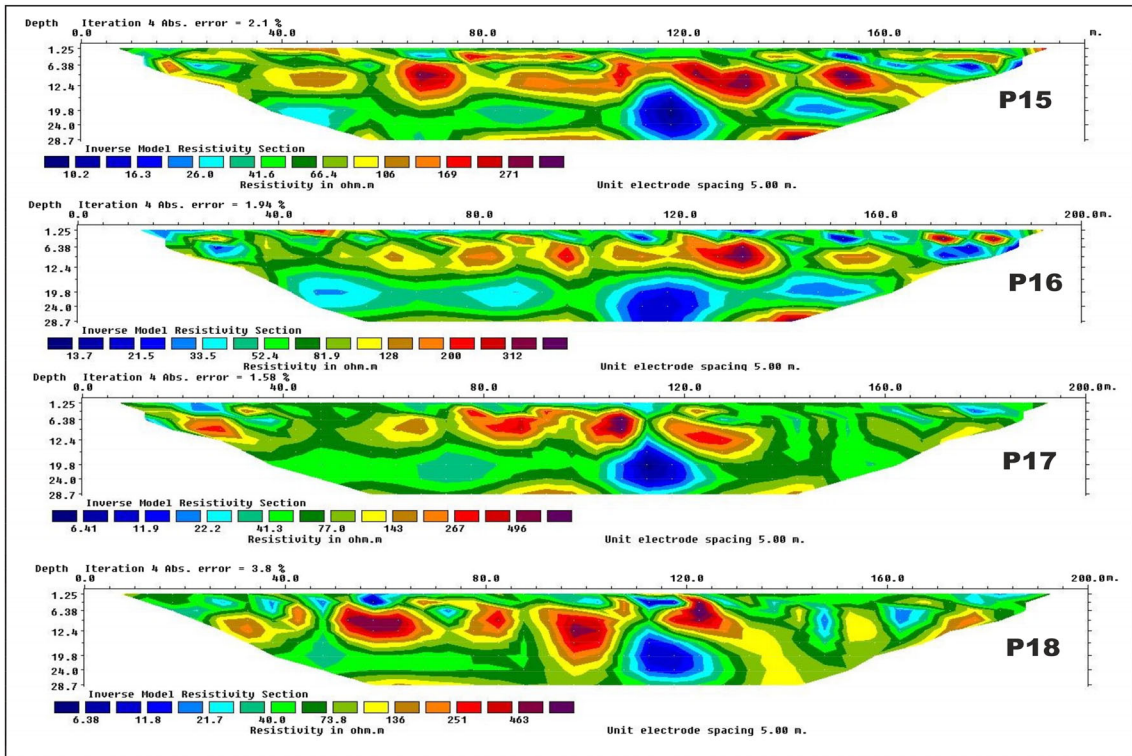
Figure 15. Two-dimensional resistivity inversion results (Dipole–Dipole array: profiles 15–18).
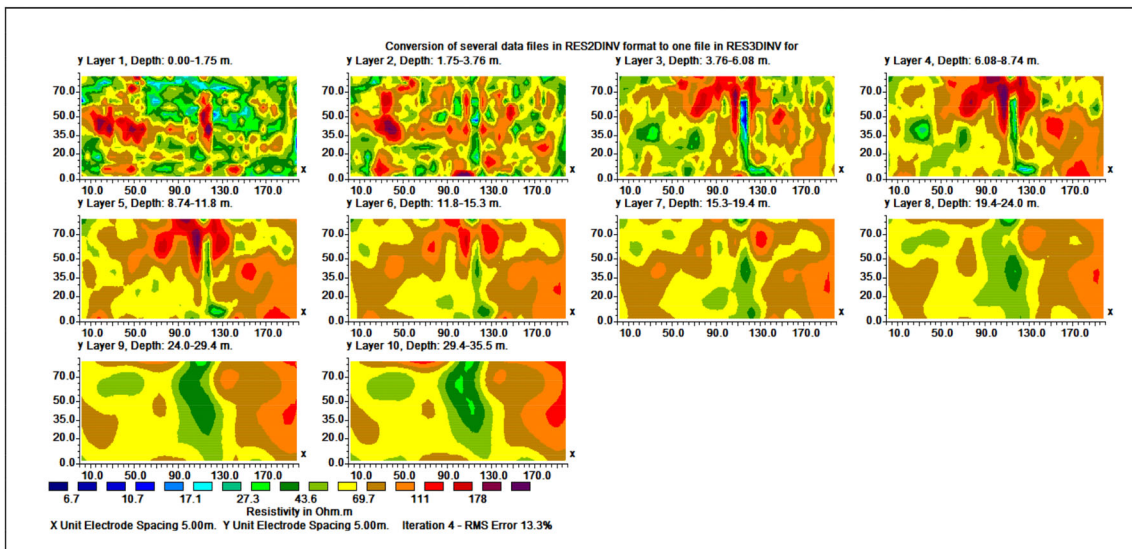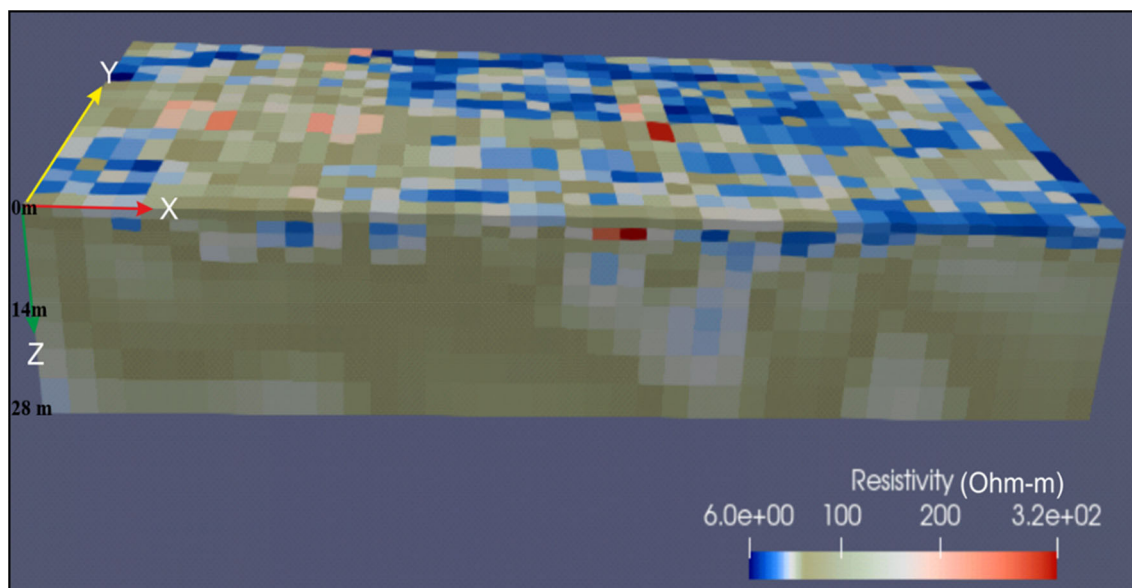

Figure 16. Three-dimensional resistivity inversion results (Dipole–Dipole array) on the *x*, *y* plane (from 0 to 24.0 m depth).

displayed the three-dimensional visualization of the distribution of resistivity in the subsurface. The laterite zones and aquifer are observed and marked in the Wenner array (Fig. 10). The reso- lution of these features decreases for the Dipole– Dipole array (Fig. 17) in shallow depth of investi- gation in layered formation.

Figure 17. Three-dimensional model (*x*, *y*, and *z* directions) showing resistivity variations for the Dipole–Dipole array.

CONCLUSIONS

The quasi-3D resistivity imaging technique was conducted successfully for deciphering groundwater potential zones in lateritic terrain of the study area. The Wenner array has given the best results in the layered structures with better resolution compared to the other arrays used in this study. For more in-depth investigation, the Wenner–Schlumberger array will help identify deeper aquifers. This 3D technique can be applied adequately in complex geological areas. However, sometimes non-availability of a large area to be survey, especially in massive urbanized areas, practical problems exist. Therefore, this technique is recommended for detailed high-resolution groundwater exploration.

High resistivity zones were observed in the study area due to the presence of laterite deposits. The resistivity distributions in the east end and west end of the profiles were quite similar. The area's central part presents significantly high resistivity values. The 2D resistivity method assumes that resistivity varies only in *x*- and *z*-directions. 3D resistivity inversion considers resistivity variations in *x*, *y*, and *z*-directions. In this way, the quasi-3D resistivity imaging technique was more beneficial for subsurface spatial and temporal characterization. Hence, quasi-3D ERT can help monitor groundwater and its contaminations based on resistivity values characterization.

AVAILABILITY OF DATA AND MATERIALS

Data will be available on request.

REFERENCES

Al-Garni, M. A., Hassanein, H. I., & Gobashy, M. (2005). Ground-magnetic survey and Schlumberger sounding for identifying the subsurface factors controlling the groundwater flow along Wadi Lusab, Makkah Al-Mukarramah, Saudi Arabia. *Journal of Applied Geophysics, 4*, 59–74.

Arkoprovo, B., Adarsa, J., & Animesh, M. (2013). *Application of remote sensing, GIS and MIF technique for elucidation of groundwater potential zones from a part of Orissa coastal tract, Eastern India*. International Science Congress Association.

Arkoprovo, B., Adarsa, J., & Prakash, S. S. (2012). Delineation of groundwater potential zones using satellite remote sensing and geographic information system techniques: A case study from Ganjam district, Orissa, India.

Aziz, N. A., Abdulrazzaq, Z. T., & Agbasi, O. E. (2019). Mapping of subsurface contamination zone using 3D electrical resistivity imaging in Hilla city, Iraq. *Environmental Earth Sciences, 78*(16), 502.

Bharti, A. K., Pal, S. K., Singh, K. K. K., Singh, P. K., Prakash, A., & Tiwary, R. K. (2019). Groundwater prospecting by the inversion of cumulative data of Wenner–Schlumberger and dipole–dipole arrays: A case study at Turamdih, Jharkhand, India. *Journal of Earth System Science, 128*(4), 107.

Bhunia, G. S., Samanta, S., Pal, D. K., & Pal, B. (2012). Assessment of groundwater potential zone in Paschim Medinipur District, West Bengal–a meso-scale study using GIS and remote sensing approach. *Assessment, 2*(5), 41–59.

Castilho, G. P., & Maia, D. F. (2008). A successful mixed land-underwater 3D resistivity survey in an extremely challenging environment in Amazônia. In *Symposium on the application of geophysics to engineering and environmental problems 2008* (pp. 1150–1158). Society of Exploration Geophysicists.

Chandra, S., Rao, V. A., Krishnamurthy, N. S., Dutta, S., & Ahmed, S. (2006). Integrated studies for characterization of lineaments used to locate groundwater potential zones in a hard rock region of Karnataka, India. *Hydrogeology Journal, 14*(6), 1042–1051.

Chowdhury, A., Jha, M. K., & Chowdary, V. M. (2009). Delineation of groundwater recharge zones and identification of artificial recharge sites in West Medinipur district, West Bengal, using RS, GIS and MCDM techniques. *Environmental Earth Sciences, 59*(6), 1209.

Dahlin, T. (2001). The development of DC resistivity imaging techniques. *Computers & Geosciences, 27*(9), 1019–1029.

Dahlin, T., Bernstone, C., & Loke, M. H. (2002). A 3-D resistivity investigation of a contaminated site at Lernacken, Sweden. *Geophysics, 67*(6), 1692–1700.

Daily, W., Ramirez, A., LaBrecque, D., & Nitao, J. (1992). Electrical resistivity tomography of vadose water movement. *Water Resources Research, 28*(5), 1429–1442.

DeGroot-Hedlin, C., & Constable, S. (1990). Occam's inversion to generate smooth, two-dimensional models from magnetotelluric data. *Geophysics, 55*(12), 1613–1624.

Dey, A., & Morrison, H. F. (1979). Resistivity modeling for arbitrarily shaped three-dimensional structures. *Geophysics, 44*(4), 753–780.

Gharibi, M., & Bentley, L. R. (2005). Resolution of 3-D electrical resistivity images from inversions of 2-D orthogonal lines. *Journal of Environmental and Engineering Geophysics, 10*(4), 339–349.

Griffiths, D. H., & Barker, R. D. (1993). Two-dimensional resistivity imaging and modelling in areas of complex geology. *Journal of Applied Geophysics, 29*(3–4), 211–226.

Griffiths, D. H., Turnbull, J., & Olayinka, A. I. (1990). Two-dimensional resistivity mapping with a computer-controlled array. *First Break, 8*(4), 121–129.

Koefoed, O. (1979). Geosounding Principles 1: Resistivity Sounding Measurements. Amsterdam: Elsevier Science Publishing Company.

Kumar, D., Mondal, S., Nandan, M. J., Harini, P., Sekhar, B. S., & Sen, M. K. (2016). Two-dimensional electrical resistivity tomography (ERT) and time-domain-induced polarization (TDIP) study in hard rock for groundwater investigation: a case study at Choutuppal Telangana, India. *Arabian Journal of Geosciences, 9*(5), 355.

Kumar, D., Rao, V. A., & Sarma, V. S. (2014). Hydrogeological and geophysical study for deeper groundwater resource in quartzitic hard rock ridge region from 2D resistivity data. *Journal of Earth System Science, 123*(3), 531–543.

Kumar, P., Tiwari, P., Biswas, A., & Acharya, T. (2020). Geophysical and hydrogeological investigation for the saline water invasion in the coastal aquifers of West Bengal, India: A critical insight in the coastal saline clay–sand sediment system. *Environmental Monitoring and Assessment, 192*(9), 1–22.

Loke, M. H. (1999). Electrical imaging surveys for environmental and engineering studies. User's Manual for Res2dinv. Electronic version available from https://geometrics.com/wp-content/uploads/2018/10/Lokenote.pdf.

Loke, M. H. (2003). Rapid 2D resistivity & IP inversion using the least-squares method. Geotomo Software. Manual.

Loke, M. H. (2004). Tutorial: 2D and 3D electrical imaging surveys. Electronic version available from https://sites.ualberta.ca/~unsworth/UA-classes/223/loke_course_notes.pdf.

Loke, M. H., & Barker, R. D. (1996). Rapid least-squares inversion of apparent resistivity pseudosections by a quasi-Newton method 1. *Geophysical Prospecting, 44*(1), 131–152.

Loke, M. H., & Dahlin, T. (2010). Methods to reduce banding effects in 3-D resistivity inversion. In *Near surface 2010–16th EAGE European meeting of environmental and engineering geophysics* (pp. cp–164). European Association of Geoscientists & Engineers.

Mondal, S. (2012). Remote sensing and GIS based ground water potential mapping of Kangshabati irrigation command area, West Bengal. *J Geogr Nat Disast, 1*(1), 1–8.

Mukherjee, A., & Sengupta, P. (2014). Project completion report on International Training Workshop on Borehole Geophysics and Groundwater. Indian Institute of Technology, Kharagpur, India.

Niyogi, D. (1975). Quaternary geology of the coastal plain of West Bengal and Orissa. *Indian Journal of Earth Science, 2*(1), 51–61.

Noel, M., & Xu, B. (1991). Archaeological investigation by electrical resistivity tomography: A preliminary study. *Geophysical Journal International, 107*(1), 95–102.

Panda, K. P., Sharma, S. P., & Jha, M. K. (2018). Mapping lithological variations in a river basin of West Bengal, India using electrical resistivity survey: Implications for artificial recharge. *Environmental Earth Sciences, 77*(17), 626.

Park, S. K., & Van, G. P. (1991). Inversion of pole-pole data for 3-D resistivity structure beneath arrays of electrodes. *Geophysics, 56*(7), 951–960.

Park, S., Yi, M. J., Kim, J. H., & Shin, S. W. (2016). Electrical resistivity imaging (ERI) monitoring for groundwater contamination in an uncontrolled landfill, South Korea. *Journal of Applied Geophysics, 135*, 1–7.

Raghunath, H. M. (2006). *Hydrology: Principles, analysis and design*. New Age International.

Sandberg, S. K., Slater, L. D., & Versteeg, R. (2002). An integrated geophysical investigation of the hydrogeology of an anisotropic unconfined aquifer. *Journal of Hydrology, 267*(3–4), 227–243.

Sasaki, Y. (1992). Resolution of resistivity tomography inferred from numerical simulation 1. *Geophysical Prospecting, 40*(4), 453–463.

Sengupta, S. (1966). Geological and geophysical studies in western part of Bengal basin, India. *AAPG Bulletin, 50*(5), 1001–1017.

Storz, H., Storz, W., & Jacobs, F. (2000). Electrical resistivity tomography to investigate geological structures of the earth's upper crust. *Geophysical Prospecting, 48*(3), 455–472.

Tardy, Y. (1992). Diversity and terminology of lateritic profiles. In *Developments in earth surface processes* (Vol. 2, pp. 379–405). Elsevier.

Tardy, Y. (1997). *Petrology of laterites and tropical soils*. AA Balkema.

Telford, W. M., Telford, W. M., Geldart, L. P., Sheriff, R. E., & Sheriff, R. E. (1990). *Applied geophysics*. Cambridge University Press.

Terrameter, L. S. (2012). Instruction manual. ABEM100709.

Usifo, A. G., Adeola, A. J., Akinnawo, O. O., & Onaiwu, K. N. (2018). Evaluation of lateritic soil using 2-d electrical resistivity methods at Alapoti, Southwestern Nigeria. *Global Journal of Pure and Applied Sciences, 24*(1), 25–36.

Yi, M. J., Kim, J. H., Song, Y., Cho, S. J., Chung, S. H., & Suh, J. H. (2001). Three-dimensional imaging of subsurface structures using resistivity data. *Geophysical Prospecting, 49*(4), 483–497.

Zhang, P. S., Liu, S. D., Wu, R. X., & Cao, Y. (2009). Dynamic detection of overburden deformation and failure in mining workface by 3D resistivity method. *Chinese Journal of Rock Mechanics and Engineering, 28*(9), 1870–1875.